Preprint typeset in JINST style - HYPER VERSION

Investigation of a direction sensitive sapphire detector stack at the $5\ GeV$ electron beam at DESY-II

O. Karacheban[ab], K. Afanaciev[c], M. Hempel[ab], H. Henschel[a], W. Lange[a], J.L. Leonard[a], I. Levy[e], W. Lohmann[bf] and S. Schuwalow[d]

[a] *Deutsches Elektronen-Synchrotron, Zeuthen, Germany*
[b] *Brandenburgische Technische Universität Cottbus, Cottbus, Germany*
[c] *NC PHEP BSU, Minsk, Belarus*
[d] *Deutsches Elektronen-Synchrotron, Hamburg, Germany*
[e] *Tel Aviv University, Tel Aviv, Israel*
[f] *CERN, Geneva, Switzerland*

E-mail: olena.karacheban@desy.de

ABSTRACT: Extremely radiation hard sensors are needed in particle physics experiments to instrument the region near the beam pipe. Examples are beam halo and beam loss monitoring systems at the Large Hadron Collider, FLASH or XFEL. Artificial diamond sensors are currently widely used as sensors in these systems. In this paper single crystal sapphire sensors are considered as a promising alternative. Industrially grown sapphire wafers are available in large sizes, are of low cost and, like diamond sensors, can be operated without cooling. Here we present results of an irradiation study done with sapphire sensors in a high intensity low energy electron beam. Then, a multichannel direction-sensitive sapphire detector stack is described. It comprises 8 sapphire plates of 1 cm^2 size and 525 μm thickness, metallized on both sides, and apposed to form a stack. Each second metal layer is supplied with a bias voltage, and the layers in between are connected to charge-sensitive preamplifiers. The performance of the detector was studied in a 5 GeV electron beam. The charge collection efficiency of the sensors was measured as a function of the bias voltage. It rises with the voltage, reaching about 10% at 950 V. The signal size obtained from an electron crossing the stack at this voltage is about 22000 e, where e is the unit charge.
Using the EUDET beam telescope, beam electrons trajectories where reconstructed, allowing to determine the position of the hits on the detector. The signal size is measured as a function of the hit position, showing variations of up to 20% in the direction perpendicular to the beam and to the electric field. The measurement of the signal size as a function of the coordinate parallel to the electric field confirms the prediction that mainly electrons contribute to the signal. Also evidence for the presence of a polarization field was observed.

KEYWORDS: Radiation-hard detectors; solid state detectors.

Contents

1. Introduction

For the operation in a harsh radiation environment, typical for near-beam detectors at LHC or free electron lasers like FLASH and XFEL, extremely radiation hard sensors are needed. Currently CVD grown diamond sensors are applied e.g. for machine induced background and on-line luminosity measurements [1, 2]. Regardless of the excellent radiation hardness and low leakage current at room temperature, the application of diamond sensors is limited due to high cost, small size and low manufacturing rate. As an alternative we suggest to use sapphire sensors. Optical grade single crystal sapphire is industrially grown in practically unlimited amount and the wafers are of large size and low cost. Sapphire sensors have been used so far in cases where the signal is generated by simultaneous hits of many particles, i.e. in the beam halo measurement at FLASH, and are planned to be installed at FLASH II and XFEL. It was found that the time characteristics of signals from sapphire sensors are similar to the ones from CVD diamond sensors [2]. The radiation hardness of sapphire sensors was studied in a low energy electron beam up to an absorbed dose of 12 MGy [3]. The charge collection efficiency, CCE, as a function of the dose will be presented. Furthermore, a detector composed of metallized sapphire plates of 10×10 mm^2 area and 525 μm thickness to be used for single particle detection is investigated in a 5 GeV electron beam. Basic characteristics, like the dependence of the CCE on the applied voltage and position resolved sensor response, are reported.

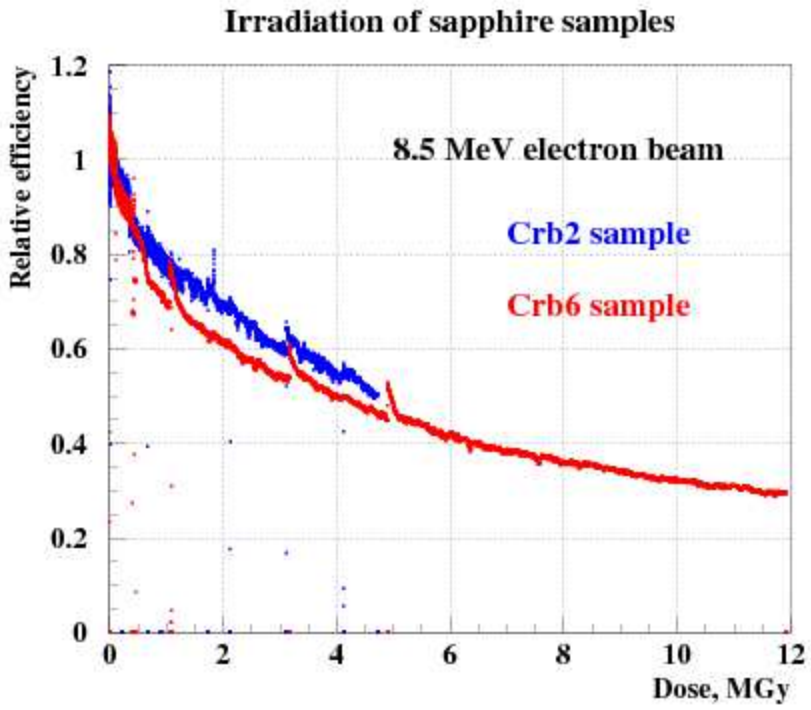

Figure 1: The relative CCE as a function of the dose in an electron beam for two sapphire sensors.

2. The response of sapphire sensors as a function of the dose

Two sensors were exposed to a high-intensity electron beam at the linear accelerator DALINAC at TU Darmstadt, Germany. The beam energy was 8.5 *MeV*, a typical value for electrons and positrons in the electromagnetic shower maximum for the near-beam calorimetry at the future linear collider [4]. The response of the sensors was measured as signal current. The relative drop of the signal current, interpreted as the relative drop of the charge collection efficiency, CCE, is shown in Figure 1 for both sensor samples. As can be seen, the CCE degrades to about 30% of the initial CCE after a dose of 12 *MGy*, corresponding to more than 10 years of operation at e.g. the ILC [5] at nominal beam parameters at 500 *GeV* centre-of-mass energy [6]. The peaks on the rather smooth curves indicate an increased CCE after periods when the beam was switched off to allow other intermediate measurements or because of beam losses. When the beam was switched back on, the CCE continued to decrease. The leakage current of the sensors was measured before and after irradiation to be below 10 pA.

3. Detector stack design

For a CCE of about 10% of industrially produced sapphire, the signal expected for particles crossing a plate of 500 μm thickness perpendicular to its surface is only about 1100 e. However, if the particle crosses the sapphire sensor parallel to the 10×10 mm^2 metallized surface, as shown in

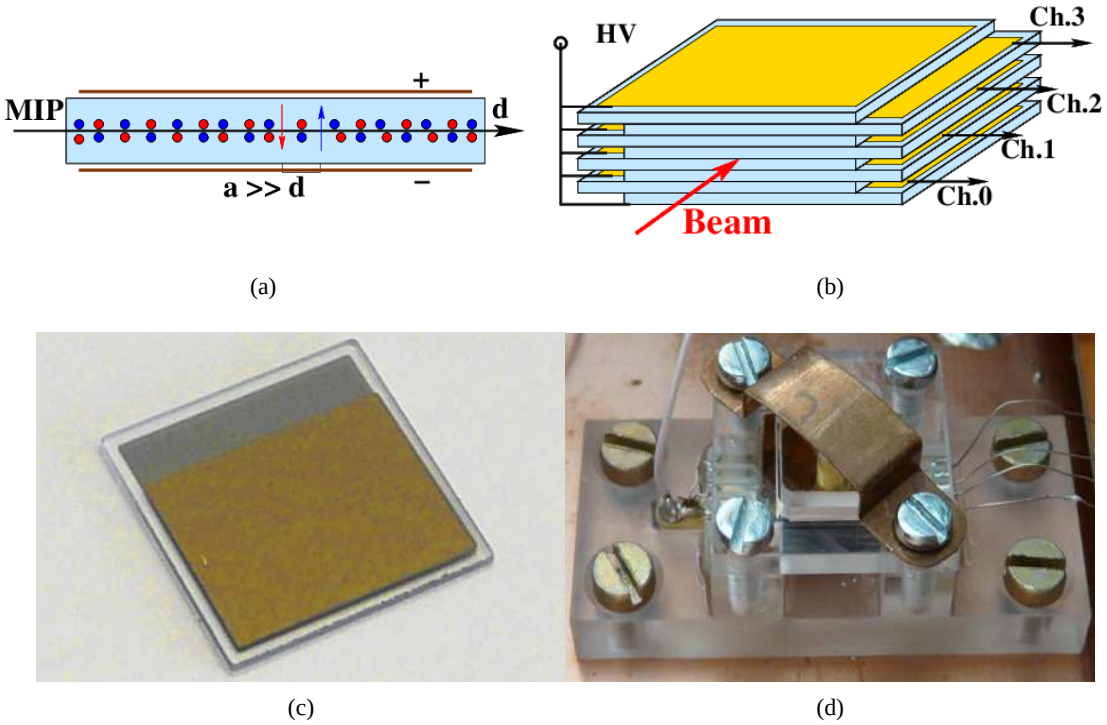

Figure 2: The sapphire detector under test: (a) – Orientation of single sapphire sensor with respect to the beam. (b) – Schematic view of detector stack consisting of eight metallized sapphire sensors. (c) – Metallized sapphire sensor. (d) – Assembled detector stack as used in the test beam.

Figure 2 (a), the signal is enhanced by a factor 20, amounting to about 22000 e, comparable to the one in currently used solid state detectors. Therefore the orientation of the sapphire plates in the test beam was chosen to be parallel to the beam direction. In addition, this orientation leads to a direction sensitivity. Only particles crossing the sensor parallel to the surface create the maximum signal. To increase the effective area of the detector, eight plates were assembled together. To allow wire bonding connections to the high voltage and to the readout electronics, the plates were alternatively shifted to both sides. Each readout channel served two plates, as can be seen in Figure 2 (b). Each sensor has dimensions $10 \times 10 \times 0.5\ mm^3$, metallized from both sides with consecutive layers of Al, Pt and Au of 50 *nm*, 50 *nm* and 200 *nm* thickness, respectively. On one side, shown on the top plate in Figure 2 (b), the metallization has a square shape of $9 \times 9\ mm^2$ area. On the opposite side the metallization area is $9 \times 7\ mm^2$ with 9 *mm* parallel to the beam direction, as shown in Figure 2 (c). This way an accidental contact of high voltage wire bonds with the readout pad on the adjacent sensor is excluded. The total height of the stack was 4.2 *mm* with 7 *mm* overlap of the metal pads, leading to a sensitive area of 29.4 mm^2. The sensors were mounted inside a plastic frame as shown in Figure 2 (d). The wire bonds for high voltage and readout connections are seen at the left and right side, respectively, in Figure 2 (b) and (d). The leakage current of each pair of sensors was measured to be below 10 *pA* at 1000 *V*.

4. Test beam setup

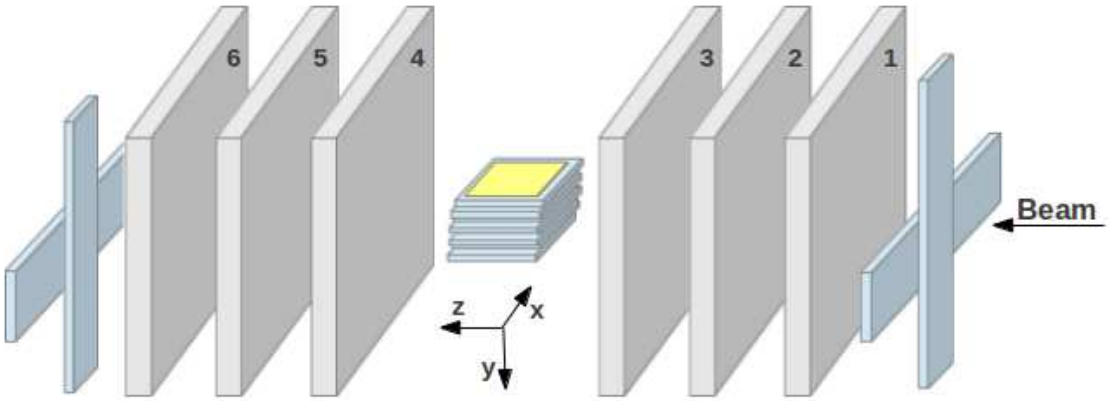

Figure 3: Sketch of the test beam setup. The sapphire stack was mounted in the middle of the 6 planes of the EUDET telescope. Crosses of two scintillators upstream and downstream of the telescope were used as the trigger for the DAQ.

The stack was mounted in the middle of six planes of the EUDET pixel telescope [7] in the 5 *GeV* electron beam of the DESY-II accelerator. Signals from sensors were amplified and shaped by charge sensitive preamplifiers A250 and standard RC-CR shapers with a peaking time of 100 *ns* and digitised by a 500 MS/s flash ADC v1721.

Two pairs of scintillators, shown as light blue planes in Figure 3 upstream and downstream of the telescope, were used as trigger to readout the telescope and the sensors. The EUDET telescope is instrumented with Mimosa26 sensors, comprising 576×1152 pixels each, with a pixel size of 18.4×18.4 μm. The telescope planes were grouped. Planes $1-3$ form the first arm, and planes $4-6$ the second arm. Tracks of beam electrons were reconstructed for each group separately. From special alignment runs the width of residual distributions was measured to be below 4 μm. From a Monte Carlo study the maximum displacement of the trajectory of a 5 *GeV* electron due to multiple scattering in the stack was estimated to be 10 μm.

5. Data synchronization and analysis

For the synchronization of the EUDET telescope and the stack readout a dedicated trigger logic unit, TLU [7], was used. For each trigger the TLU distributed a trigger sequence to the EUDET telescope and the stack data acquisitions, such that a unique correspondence between records from both readouts was ensured.

The standard telescope analysis software [7] was used to convert hits in the EUDET telescope into space-points in the user geometry with the origin of the coordinate system as shown in Figure 3.

Events with more than one track candidate in the telescope, amounting to about 30%, were rejected. For the remaining events the track fit was done separately for the first and second arm of the telescope. The two reconstructed tracks are considered to originate from the same beam

electron if their distance in the $z = 0$ plane was less than a predefined cut. To determine the precise position of the stack in the beam, events with a large angle between the tracks of the first and second telescope arm were used. Requiring this angle to be larger than 0.5 *mrad*, an image of the stack in the *xy* plane at $z = 0$ is obtained, as shown in Figure 4. From the precise position of each plate geometrical cuts were applied to select hits in each readout channel separately. Counting plates in Figure 4 from top to bottom, the top two plates correspond to readout channel 0.

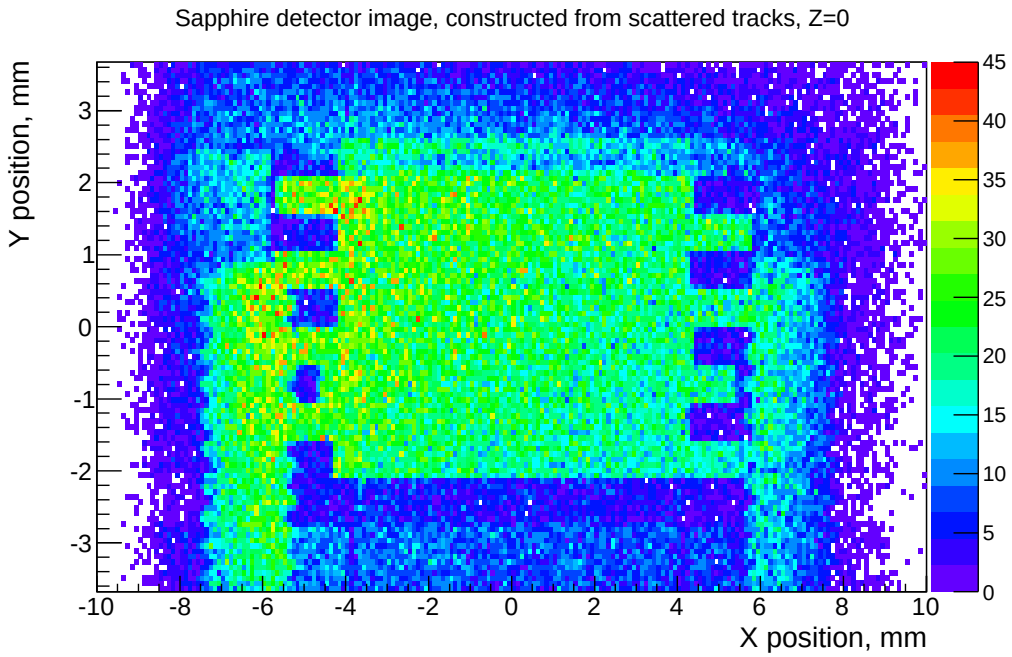

Figure 4: The image of the stack, obtained selecting tracks reconstructed in the first and second telescope arm with an angle larger than 0.5*mrad*. Counting plates from top to bottom, the two top plates correspond to readout channel 0 and the two bottom plates to readout channel 3.

For tracks, pointing into the detector active area, signals from the ADC were averaged over a large number of triggers. Events with tracks not pointing into detector were used to study common mode noise. Correlation between baseline values were investigated for all combinations of channels using the baseline values calculated in a predefined time window. These correlations were used in the further analysis for common mode noise subtraction. The averaged ADC output assigned to tracks not pointing into the detector was used to subtract the baseline from the averaged signal. As an example, the results for bias voltages of 550 *V* and 950 *V* are shown in Figure 5.

6. Charge collection efficiency

The CCE is defined as ratio of the measured to the expected signal charge. The signal charge is obtained by the integration of the ADC output over a 50 *ns* time interval in the range [420; 470] *ns*. This time interval is less than the signal length as shown in Figure 5, but the RMS of the common

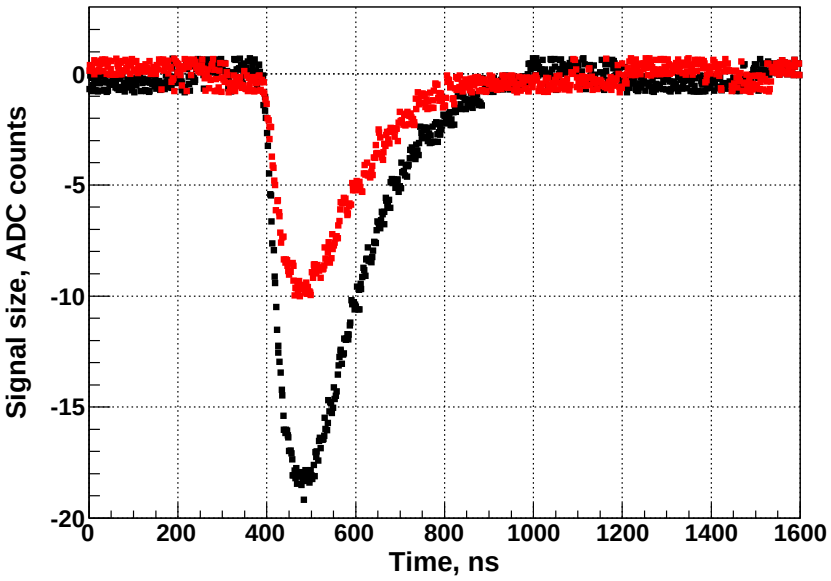

Figure 5: The averaged signal at 550 V in red and at 950 V in black for events with tracks hitting the active area of the stack after common noise subtraction.

mode noise in this range is low in comparison to the one in the tail of the signal. The mean value of the distribution of the signal charge was used for the CCE calculation at each bias voltage value.

In order to convert the mean value into a charge each channel was calibrated by injecting a known charge into the preamplifier input. The expected amount of generated electron-hole pairs is estimated from the mean value of the ionisation energy loss inside the sensor, obtained from a GEANT [8] simulation, and the energy needed to create an electron-hole pair. The latter, amounting to 27 eV, is estimated using the extrapolation proposed in Ref. [9], corrected for wide band-gap semiconductors [10].

The measured CCE is shown in Figure 6 as a function of the bias voltage for all plates of the stack. For each voltage value a statistics of 100000 triggers was used. To avoid an influence of metallization edges only the central part of stack was used for CCE calculation, $-3\ mm < x < 3\ mm$. An almost linear rise of the CCE is observed, reaching at 950 V e.g. for plane 1 a value of 10.5%. The values of the CCE obtained for all plates at a voltage of 950 V are listed in the Table 1. The statistical error is obtained as the standard deviation of the mean value. The systematic uncertainty is the uncertainty due to the calibration and the uncertainty due to edge effects in the y coordinate, added in quadrature. The measured CCE varies from sample-to-sample reflecting variation of the substrate quality. As can be seen, 5 out of the 8 sensor plates have a relatively high and similar CCE of about $7-10\%$, while three other plates have lower and different CCE values. A quantity <CCE> was defined as the averaged value of 12 CCE measurements for each plate in 500 μm steps of the x coordinate. Its values are given together with the RMS in Table 1. The CCE obtained from the voltage scan at 950 V and the average <CCE> are in agreement within the uncertainties of the

Plate number	1	2	3	4	5	6	7	8
CCE, %	10.5	7.4	9.5	8.6	8.1	5.3	3.6	2.2
Stat. error	0.3	0.2	0.2	0.2	0.2	0.1	0.1	0.1
Syst. error	0.2	0.2	0.2	0.2	0.2	0.1	0.1	0.1
<CCE>, %	9.9	7.2	9.0	8.5	7.5	5.3	3.7	2.1
RMS	1.7	0.9	0.9	0.8	0.6	0.5	0.9	0.7

Table 1: The measured CCE at the highest applied bias voltage of 950 V with statistical and systematic uncertainties. Also given are the quantities <CCE> and RMS obtained from averaging CCE measurements in 500 μm steps in the x coordinate.

measurements.

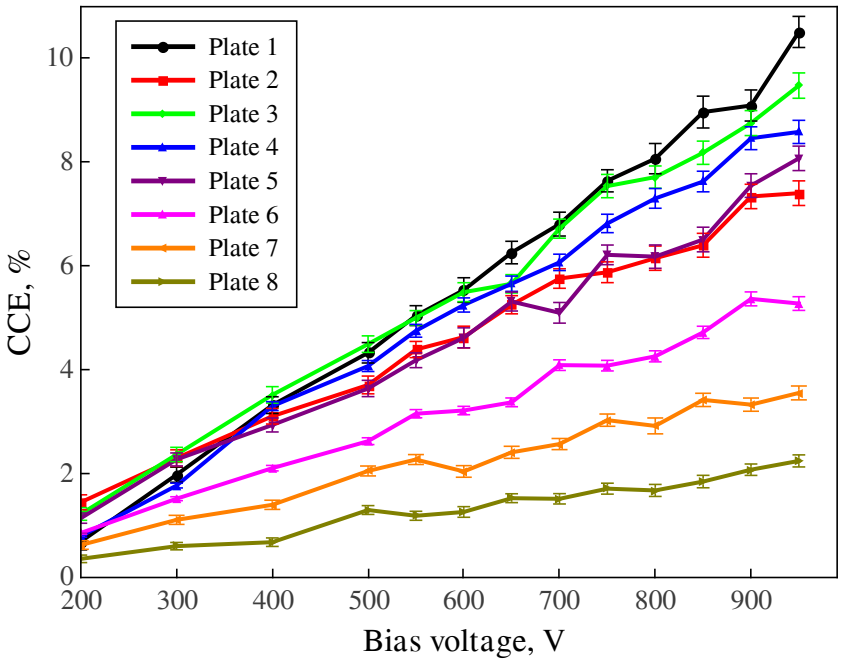

Figure 6: Measurement of the mean charge collection efficiency for eight sapphire plates as a function of the bias voltage.

7. Theoretical model for the charge collection efficiency of sapphire sensors

A linear model was developed to describe the CCE as a function of the local y coordinate inside a plate.

Charged particles cross the sensor and ionize the atoms along their path through the sensor of thickness d. N_0 electron-hole pairs are produced. Some charge carriers will recombine immediately. A fraction of both types of charge carriers, called f_d, start to drift to the corresponding electrodes when an external electric field is applied. During the drift charge carriers may be trapped

Plate number	B, $V/\mu m$	f_d, %	$\mu\tau(e)$, $\mu m^2/V$	$\mu\tau(h)$, $\mu m^2/V$	χ^2
1	1.327 ± 0.012	52.9 ± 0.5	79.1 ± 1.1	4.2 ± 0.3	19
2	1.255 ± 0.011	47.1 ± 0.5	59.5 ± 0.9	6.2 ± 0.3	41
3	1.307 ± 0.010	53.3 ± 0.5	64.9 ± 0.9	6.4 ± 0.2	27
4	1.287 ± 0.011	48.1 ± 0.5	74.6 ± 1.0	3.3 ± 0.3	27
5	1.421 ± 0.010	47.1 ± 0.7	62.9 ± 1.0	3.2 ± 0.4	16
6	1.342 ± 0.013	43.5 ± 1.3	39.4 ± 1.2	5.1 ± 0.4	42
7	1.484 ± 0.010	50.1 ± 1.2	22.0 ± 0.8	3.7 ± 0.4	19
8	1.330 ± 0.010	40.7 ± 1.7	15.1 ± 0.5	3.2 ± 0.4	33

Table 2: Fit parameters for the case of electrons and holes contribution.

and released only after some time which leads to the reduction of their contribution to the observed signal pulse. If the occupation of traps is small and detrapping time is significantly shorter than the duration of the measurement, the density of trapped charges in steady state will be proportional to the flux of drifting charge carriers. The space charge due to trapped charges generates an internal electric field, called polarization field, with the direction opposite to the externally applied field. Assuming that the space charge density will be a linear function of the local y, the resulting electric field has a parabolic shape, in the simplest case of a non-charged crystal $E(y) = A(y - \frac{d}{2})^2 + B$, where A and B are parameters. The integral of the electric field over the full sensor thickness d is equal to the bias voltage.

To estimate the signal size electrons and holes will be considered separately, as they may contribute to the resulting signal differently. The drift velocity $v_{e,h}$ is assumed to be directly proportional to the electric field strength, $v_{e,h} = \mu_{e,h}E(y)$, where $\mu_{e,h}$ is the mobility for electrons and holes, respectively.

The charge carrier lifetime $\tau_{e,h}$ is assumed to be constant. Then the number of carriers at time t is $N_{e,h}(t) = f_d \cdot N_0 e^{-t/\tau_{e,h}}$. According to Ramo's theorem the differential contribution to the observed signal is $dQ = \frac{e}{d}N(t)v_{e,h}dt$. Substituting dt by $dt = \frac{dy}{\mu_{e,h}E(y)}$ and integrating from the carrier generation point y_0 to the detector edge, the signal charge is parametrised as:

$$Q(y_0) = \frac{e \cdot f_d \cdot N_0}{d} \mathrm{e}^{\frac{arctan\left((y_0 - \frac{d}{2})\sqrt{\frac{A}{B}}\right)}{\mu\tau\sqrt{AB}}} \int_{y_0}^{d} \mathrm{e}^{-\frac{arctan\left((y - \frac{d}{2})\sqrt{\frac{A}{B}}\right)}{\mu\tau\sqrt{AB}}} \mathrm{d}y. \tag{7.1}$$

The quantity B is the electric field strength at the plane in the middle of the plate, $y = d/2$, and $\mu\tau$ is the drift path length of the electrons or holes in the electric field of unit strength. The ratio Q/N_0 is then the fraction of the charge carriers contribution to the observed CCE. In case of $\mu\tau E \ll d$ the proportionality between the charge carrier drift path and electric field strength leads to the linear dependence of the CCE on the detector bias voltage, in good agreement with the measurement shown in Figure 6.

Figure 7 shows the CCE as a function of the local y coordinate, measured in 25 μm slices, together with a fit using equation (7.1). The electric field has opposite direction for adjacent plates. For example, $y = 0$ μm of plate 1 and $y = 525$ μm of plate 2 correspond to the same readout electrode. In plates 1, 3, 5 and 7 the electric field is directed from $y = 525$ μm to $y = 0$ μm and

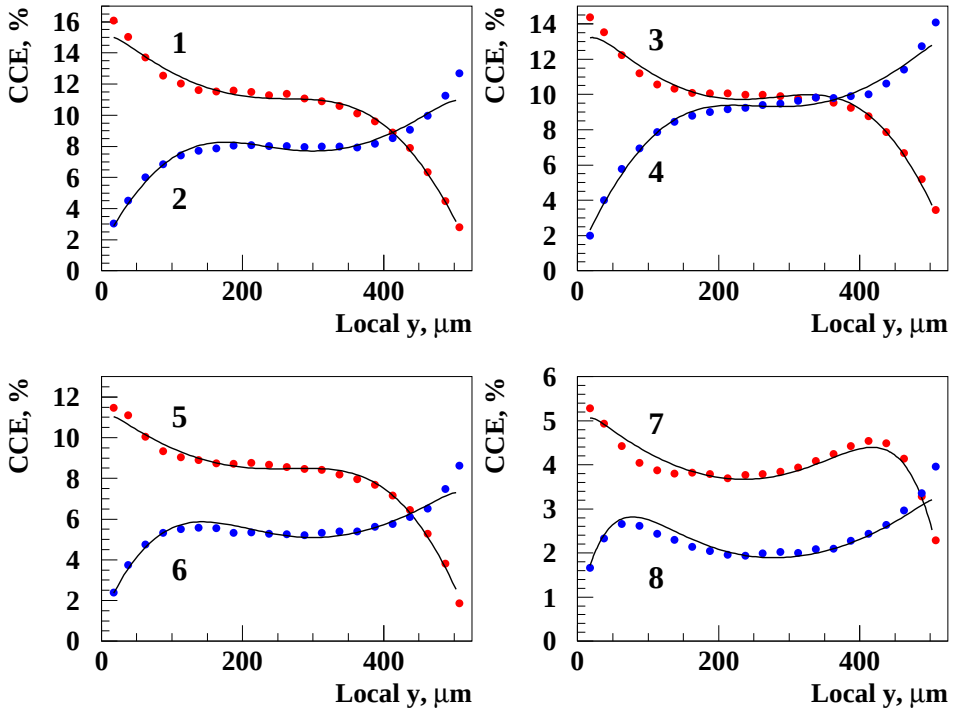

Figure 7: The CCE measured as a function of the local y coordinate inside a plate in slices of 25 μm for all plates of the sapphire stack. Blue dots are for the electric field in the direction of y and red dots for the opposite field direction. The lines are the result of a fit including both electron and hole drift. The fit parameters are given in Table 2.

the CCE is shown in red dots. In plates 2, 4, 6 and 8 the field direction is opposite, and the CCE is shown in blue dots. The parameters of the fit are listed in the Table 2. As can be seen, the drift length of electrons is in most of the cases more than 10 times larger than the drift length of the holes at roughly the same field strength. This result is consistent with low hole mobility predicted in Ref. [11] and confirms the dominant contribution of electrons for the charge transport in sapphire [12, 13].

8. Conclusions and outlook

The paper presents results of the performance of a multi channel sapphire stack, designed for single particle detection, in a 5 *GeV* electron beam. The CCE shows a linear dependence on the bias voltage reaching up to 10% at 950 V. A measurement of the CCE as a function of the local y coordinate through the thickness of the plates shows a pronounced dependence on y. The measurement can be explained by a linear model pointing to a dominant contribution of electron

drift to the signal charge and polarisation inside the bulk of the sensor. In addition, a fraction of charge carriers of about 50% recombines immediately after creation.

These results will be used for the design of next generation sapphire detector with non-uniformity compensation.

9. Acknowledgments

This work was supported by the Commission of the European Communities under the 7th Framework Program AIDA, contract no. 261015. The Tel Aviv University and the Brandenburgische Technische Universität Cottbus are supported by the German-Israel Foundation (GIF). We are grateful to the crew and the management of the S-DALINAC accelerator at the Technical University of Darmstadt for their great support during the measurements at the electron beams. The measurements leading to these results have been performed at the Test Beam Facility at DESY Hamburg (Germany), a member of the Helmholtz Association (HGF). We would also like to thank the Target Lab of the GSI Helmholtzzentrum für Schwerionenforschung for the metallization of the sensors.

References

[1] A. Bell et al., *Fast Beam Conditions Monitor BCM1F for the CMS Experiment*, Nucl.Instrum.Meth. A614 (2010) 433-438, DOI: 10.1016/j.nima.2009.12.056, M. Mikuz et al., *Diamond pad detector telescope for beam conditions and luminosity monitoring in ATLAS*, Nucl.Instrum.Meth. A579 (2007) 788-794, DOI:10.1016/j.nima.2007.05.297, Ch. Ilgner et al., *The Beam Conditions Monitor of the LHCb Experiment*, e-Print: arXiv:1001.2487, S. Sfyrla et al., *Beam Condition Monitoring with Diamonds at CDF*, IEEE Trans.Nucl.Sci. 55 (2008) 328-332, DOI: 10.1109/TNS.2007.913492.

[2] A. Ignatenko, *Beam Halo Monitor for FLASH and the European XFEL*, IPAC-2012 New Orleans, Conf.Proc. C1205201 (2012) 816-818.

[3] S. Schuwalow, *Radiation hardness studies with relativistic electrons*, Talk at 2nd CARAT Workshop, GSI, Darmstadt, 2010.

[4] Ch. Grah et al., *Polycrystalline CVD diamonds for the beam calorimeter of the ILC*, IEEE Trans.Nucl.Sci. 56 (2009) 462-467, DOI: 10.1109/TNS.2009.2013853.

[5] B.Barish et al., *The International Linear Collider Technical Design Report*, ILC-REPORT-2013-040, arXiv:1306.6327.

[6] H. Abramowicz et al., *Forward Instrumentation for ILC Detectors*, JINST 5 (2010) P12002, DOI: 10.1088/1748-0221/5/12/P12002.

[7] J. Behr, *Test Beam Measurements with the EUDET Pixel Telescope*, EUDET-Report-2010-01, Hamburg, 2010.

[8] R. Brun et al., Preprint CERN-DD/EE/84-1 (1984), revised 1985.

[9] C.A. Klein, J.Aappl.Phys., 39, 2029 (1968), DOI:10.1063/1.1656484.

[10] A.Owens, *Compound Semiconductor Radiation Detectors*, p.398, CRC Press 2012, ISBN: 9781439873137.

[11] Yong-Nian Xu and W.Y. Ching, Phys. Rev. B 43, 4461 (1991), DOI: 10.1103/PhysRevB.43.4461.

[12] R.C. Hughes, Phys. Rev. B 19, 5318 (1979); DOI: 10/PhysRevB.19.5318.

[13] U.E.Hochuli, Phys. Rev. 133, A 468 (1964); DOI: 10.1103/PhysRev.133.A468.